Torque Ripple Prediction using Fourier Coefficients of Flux Linkage in PMSM Design

Bonkil Koo[1], Ilsu Jeong[1], Kwanghee Nam[1], *Member, IEEE*, and Jeongki Kwon[2]

[1] Dept. of EE, POSTECH, 77, Cheongam-ro, Nam-gu, Pohang, 790-784 Republic of Korea, kwnam@postech.ac.kr
[2] Hyundai MOBIS, 17-2, Mabuk-ro 240, Giheung-gu, Yongin, 446-912 Republic of Korea.

To derive an estimate of torque ripple in permanent magnet synchronous motor (PMSM), analytic expression of torque is developed using the stator flux linkages. The flux linkage data are obtained from FEM analysis, and they are expressed as Fourier series after a dq transformation. Further, the torque equation is obtained using the Fourier coefficients and the first three harmonic components (6^{th}, 12^{th}, 18^{th}) are used to make a torque ripple estimate. Through comparison studies, it is shown that the prediction matches well with the FEM results. The prediction may be used as a guide for reducing the torque ripple at the motor design stage.

***Index Terms*—Finite element analysis, Fourier series, permanent magnet machines.**

I. Introduction

A PMSM with high saliency ratio tends to have a large torque ripple [1]. To suppress the torque ripple, step skewing is generally utilized [2]. However, a best effort is exercised to reduce torque ripple by adjusting positions of flux barriers in the design stage [3], [4]. Jeong and Nam [5] expressed torque ripple analytically utilizing the Fourier series expansion of flux linkages. In this work, the magnitude trend of torque ripple is predicted by using the harmonic components of the flux linkage.

II. Torque Ripple Analysis using Flux Linkages

The ISG under study has the following specifications: starting torque; 43.0 Nm, continuous rated torque; 11.5 Nm, maximum speed; 18000 rpm, maximum torque ripple; less than 10 %, and dc link voltage of the inverter; 42 V_{DC}.

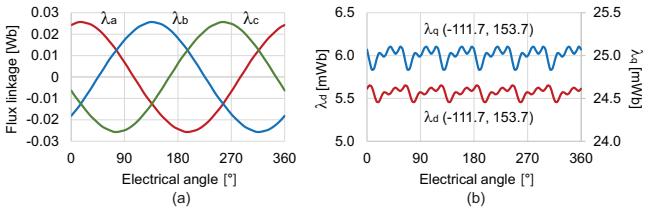

Fig. 1. Flux linkage at the rated current in (a) abc-frame and (b) synchronous dq-frame.

The flux linkages, $(\lambda_a, \lambda_b, \lambda_c)$ in the abc-frame are obtained by FEM simulation as shown in Fig. 1 (a). The simulation was performed at a rated condition: current magnitude $I_s = 190$ A, current angle $\beta = 36°$, and speed $\omega_m = 209.4$. The flux linkages are transformed into a stationary dq-frame via $\lambda_d + j\lambda_q = \frac{2}{3}\left(\lambda_a + e^{j\frac{2\pi}{3}}\lambda_b + e^{j\frac{4\pi}{3}}\lambda_c\right)$. Fig. 1 shows an example dq-fluxes corresponding to $(\lambda_a, \lambda_b, \lambda_c)$. The fundamental components of (λ_d, λ_q) are dc, since the currents are fed synchronously to the motor speed. But they have ripples caused by stator slotting and rotor field harmonics. The ripples in (λ_d, λ_q) are interpreted as the main sources causing torque ripples, thereby the ripples need to be analyzed.

We take the Fourier transform of (λ_d, λ_q) with respect to the geometric angle, θ_m:

$$\lambda_d(i_d, i_q, \theta_m) = \sum_{\nu=0}^{\infty} \chi_d^{(\nu)}(i_d, i_q)\cos\left(6\nu p\theta_m + \phi_d^{(\nu)}\right), \tag{1}$$

$$\lambda_q(i_d, i_q, \theta_m) = \sum_{\nu=0}^{\infty} \chi_q^{(\nu)}(i_d, i_q)\sin\left(6\nu p\theta_m + \phi_q^{(\nu)}\right), \tag{2}$$

where ν is the multiple number of the 6^{th} harmonic order, p is pole pair, i_d and i_q are d- and q-axis currents, $\chi_d^{(\nu)}$ and $\chi_q^{(\nu)}$ are Fourier coefficients, and $\phi_d^{(\nu)}$ and $\phi_q^{(\nu)}$ are phase angles corresponding to 6ν harmonics. Note that only the harmonics of multiples of 6^{th} remain in a three phase machine when there is no unbalance among phases. Nonlinearity becomes significant as the current magnitude increases due to core saturation and armature reaction. Such nonlinearity with current is reflected in the Fourier coefficients by denoting $\chi_d^{(\nu)}$ and $\chi_q^{(\nu)}$ as functions of i_d and i_q. To obtain functional description with respect to i_d and i_q, the above process must be repeated for all (i_d, i_q) in the current operation range. A methodology to obtain approximate functions was appeared in [5].

From the flux linkage, torque is represented as:

$$\begin{aligned}\hat{T} &= \frac{3}{2}p\left[\hat{\lambda}_d i_q - \hat{\lambda}_q i_d + i_d\frac{\partial\hat{\lambda}_d}{\partial\theta_m} + i_q\frac{\partial\hat{\lambda}_q}{\partial\theta_m}\right] - \frac{\partial W_m}{\partial\theta_m} \\ &= \frac{3}{2}p\sum_{\nu=0}^{3}\Big[\chi_d^{(\nu)}(i_d, i_q)\cos\left(6\nu p\theta_m + \phi_d^{(\nu)}\right)i_q \\ &\quad -\chi_q^{(\nu)}(i_d, i_q)\sin\left(6\nu p\theta_m + \phi_q^{(\nu)}\right)i_d \\ &\quad -6\nu p\chi_d^{(\nu)}(i_d, i_q)\sin\left(6\nu p\theta_m + \phi_d^{(\nu)}\right)i_d \\ &\quad +6\nu p\chi_q^{(\nu)}(i_d, i_q)\cos\left(6\nu p\theta_m + \phi_q^{(\nu)}\right)i_q\Big] - \frac{\partial W_m}{\partial\theta_m},\end{aligned} \tag{3}$$

where $\hat{\lambda}_d$ and $\hat{\lambda}_q$ are approximations of λ_d and λ_q in (1), (2) obtained by truncating high order terms $\nu \geq 4$, and $\frac{\partial W_m}{\partial\theta_m}$ is the cogging torque. Note that $\hat{\lambda}_d i_q - \hat{\lambda}_q i_d = \psi_m i_q + (L_d - L_q)i_d i_q$ in the linear model, where ψ_m is a back-EMF constant, and L_d and L_q are d- and q-axis inductances, respectively. It is the main torque component containing a dc term, whereas the

others describe ripple components. We group the d- and q-axis components of the same harmonic numbers:

$$T_0 = \left|\frac{3}{2}p\left(\hat{\lambda}_d i_q - \hat{\lambda}_q i_d\right) - T_{av}\right|, \quad (4)$$

$$T_\nu = \frac{3}{2}p \cdot 6\nu p \times \sqrt{(\chi_d^{(\nu)} i_d)^2 + (\chi_q^{(\nu)} i_q)^2 - 2\chi_d^{(\nu)}\chi_q^{(\nu)} i_d i_q \sin(\phi_q^{(\nu)} - \phi_d^{(\nu)})}$$
$$\text{for } \nu = 1, 2, 3, \quad (5)$$

where T_{av} is the average torque. In deriving (5) the cosine law is applied. T_0 represents a ripple contained in the primary dc component, while T_1, T_2, T_3 do ripple components caused by $6^{th}, 12^{th}, 18^{th}$ flux harmonics, respectively. Fig. 2 shows ripple components, T_0, T_1, T_2, and T_3 when current magnitudes and current angles are (I_s, β)= (280, 0°), (190, 36°), and (90, 70°). It shows that the 6^{th} harmonic is the most influential in all cases.

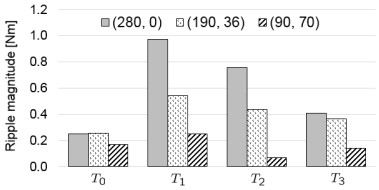

Fig. 2. Torque ripple magnitudes, T_0, T_1, T_2, and T_3 when the currents are (I_s, β) = (280, 0°), (190, 36°), and (90, 70°).

As a torque ripple estimate, it is proposed here to use the sum up to 18^{th} order:

$$\mathcal{M} \triangleq T_1 + T_2 + T_3. \quad (6)$$

Note that $\mathcal{M}$ represents the sum of the harmonic powers of 6^{th}, 12^{th}, and 18^{th}.

III. Torque Ripple Suppression Design

Fig. 3 shows a sectional view of the ISG motor which has 8-pole, 72-slot, and delta-type magnet arrangement. Two flux barrier angles, γ and δ are selected as design parameters for suppressing torque ripple, while the other variables such as magnet lengths and positions were fixed. It is observed that the torque ripple is sensitive to the flux barrier location determined by γ and δ.

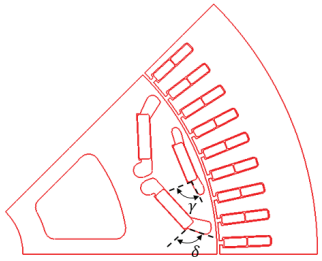

Fig. 3. Sectional view of the ISG motor and design parameters, γ and δ.

To find the ripple minimizing solution, FEM analysis was performed by varying γ and δ from 90° to 108° and from 90° to 135°, respectively. At the same time, we calculated $\mathcal{M}$ for each design following the procedure illustrated in the above section. Fig. 4 shows that the ripple trends when γ and δ change at a rated condition, (I_s, β)=(190, 36°). Note that the FEM results and the ripple prediction by $\mathcal{M}$ have similar trends.

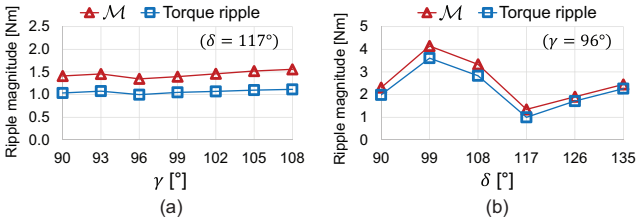

Fig. 4. Trends of $\mathcal{M}$ and torque ripple (FEM results) at a rated condition, (I_s, β)=(190, 36°) versus (a) γ and (b) δ.

To study $\mathcal{M}$ as an indication of torque ripple, comparison analysis was done extensively. Fig. 5 shows contours of $\mathcal{M}$ and torque ripples obtained by FEM simulation over the γ—δ plane. They agree in general, and in finding a minimizing solution, $\gamma = 96°$ and $\delta = 117°$.

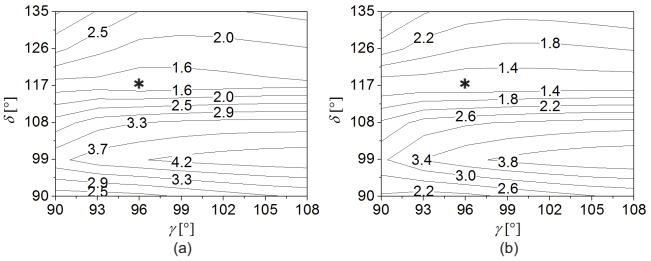

Fig. 5. Contours: (a) $\mathcal{M}$ and (b) torque ripple (FEM) at (I_s, β)=(190, 36°).

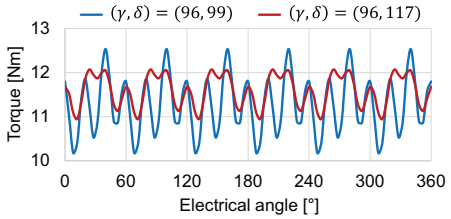

Fig. 6. Torque ripple waveform when the $(\gamma, \delta) = (96, 99)$ and $(\gamma, \delta) = (96, 117)$.

Fig. 6 shows sample torque ripples versus angle for $(\gamma, \delta) = (96, 99)$ and $(\gamma, \delta) = (96, 117)$. The ripples are 20.9% and 9.7%, respectively.

References

[1] A. Fratta, G. P. Troglia, A. Vagati, and F. Villata, "Evaluation of Torque Ripple in High Performance Synchronous Reluctance Machines," in *Conf. Rec. IEEE IAS Annu. Meeting*, Toronto, Ont., Canada, vol. 1, pp. 163-170, Oct. 1993.

[2] W. Q. Chu, Z. Q. Zhu, "Investigation of Torque Ripples in Permanent Magnet Synchronous Machines With Skewing," *IEEE Trans. on Magn.*, vol. 49, no. 3, pp. 1211-1220, Mar. 2013.

[3] A. Vagati, M. Pastorelli, G. Franceschini, and S. C. Petrache, "Design of Low-Torque-Ripple Synchronous Reluctance Motors," *IEEE Trans. on Ind. Appl.*, vol. 34, no. 4, pp. 758-765, Jul./Aug. 1998.

[4] N. Bianchi, S. Bolognani, D. Bon, M. D. Pre, "Rotor Flux-Barrier Design for Torque Ripple Reduction in Synchronous Reluctance and PM-Assisted Synchronous Reluctance Motors," *IEEE Trans. on Ind. Appl.*, vol. 45, no. 3, pp. 921-928, May/Jun. 2009.

[5] Iisu Jeong, Kwanghee Nam, "Aanlytical Expression of Troque and Inductances via Polynomial Approximations of Flux Linkages," under review for *IEEE Trans. on Magn.*, 2015.